Chemical Engineering Journal 429 (2022) 131751

Contents lists available at ScienceDirect

Chemical Engineering Journal

journal homepage: www.elsevier.com/locate/cej

The new tailored nanoporous carbons from the common polypody (*Polypodium vulgare*): The role of textural properties for enhanced CO_2 adsorption

Jarosław Serafin [a], Karolina Kiełbasa [b], Beata Michalkiewicz [b,*]

[a] *Institute of Energy Technologies, Department of Chemical Engineering and Barcelona Research Center in Multiscale Science and Engineering, Universitat Politècnica de Catalunya, EEBE, Eduard Maristany 10-14, 08019 Barcelona, Spain*

[b] *West Pomeranian University of Technology in Szczecin, Faculty of Chemical Technology and Engineering, Department of Catalytic and Sorbent Materials Engineering, Piastów Ave. 42, 71-065 Szczecin, Poland*

ARTICLE INFO

Keywords:
Biomass
Nanoporous carbons
Common polypody
CO_2 adsorption
CO_2/N_2 selectivity
Adsorption isotherms

ABSTRACT

The one-step synthesis of new tailored nanoporous carbons (NCs) from the common polypody (*Polypodium vulgare*) as feedstock for the first time was presented. The significance of nitrogen flow (2.25 – 30 dm^3/h) and temperature (500 – 900 °C) during carbonization was investigated. KOH activated NCs have a high specific surface area (1994 m^2/g), large total pore volume (0.998 cm^3/g), and micropore volume (0.923 cm^3/g). NCs displayed tailored textural properties for CO_2 capture. The NCs showed superior CO_2 adsorption at 1 bar equal to 5.67 and 9.05 mmol/g, for 298 and 273 K, respectively. The selectivity of CO_2 adsorption in relation to N_2 was also high. The selectivity coefficient was achieved to 23 and S_{IAST} selectivity 59.5. The isosteric heat of adsorption calculated on the basis of the Clausius-Clapeyron equation and Sips model was ranged from 26 to 31 kJ/mol and suggested the physisorption mechanism of adsorption.

1. Inroduction

Both industrial and energy production currently require the fossil fuels burring of on a large scale [1]. Fossil fuel combustion is responsible for over 50% of greenhouse gas emissions [2]. Hence the CO_2 reduction is necessary for humans and all life on earth. In recent decades, reducing anthropogenic CO_2 emissions has attracted growing attention and is extremely urgent to relax from global warming [3]. Many technologies can be applied to separate CO_2 from a gas mixture. They represent the following types of processes: absorption [4], physical adsorption [5,6,7], chemical adsorption [8], cryogenic separation [9] and membranes [10].

Only chemical absorption (the amine-based absorption) is a mature carbon dioxide removing process and is the most common technology. Still, there are many problems associated with the amine-based absorption technology: high level of energy consumption, corrosion of equipment, degradation of the amines solutions, excessive evaporative losses of amines, and possible formation of toxic by-products [11]. Considering the limitations of the amine-based absorption process solid porous materials are more attractive for CO_2 capture because the entire process is energy-efficient, easily reversible, environmentally friendly [12,13].

Lately a lot of various solid materials have been tested as solid sorbents: porous carbons [14,15,16], metal–organic frameworks (MOFs) [17], zeolites [18], polymers [19], TiO_2 [20], CaO [21], $CaCO_3$ [22]. Among these solid sorbents, the superior adsorption capacity has been described for microporous activated carbons [13,14,23,24]. Activated carbon (ACs) can be produced from any carbonaceous material. ACs producet from MOFs [25,26], polydopamine [27,28], polypyrrole [29,30], porous aromatic framework [31], benzimidazole [32], revealed excellent adsorption capacity. Unfortunately this approach is way too expensive for large-scale use. Porous carbon produced from fungi [33], chitosan [34] and Novus pallet scrap [35] were described as very good and selective sorbents for CO_2. Natural biomass, is a promising alternative carbon source because of its great abundance, price and sustainability. However, it should be taken into account that much of natural biomass are valuable food or industrial feedstock.

Herein, we disclose the one-step synthesis combining carbonization and chemical activation stages utilizing common polypody leaves as a carbon precursor and KOH as an activating agent to design highly

* Corresponding author.
E-mail address: beata.michalkiewicz@zut.edu.pl (B. Michalkiewicz).

https://doi.org/10.1016/j.cej.2021.131751
Received 18 June 2021; Received in revised form 3 August 2021; Accepted 6 August 2021
Available online 20 September 2021
1385-8947/© 2021 The Author(s). Published by Elsevier B.V. This is an open access article under the CC BY license (http://creativecommons.org/licenses/by/4.0/).

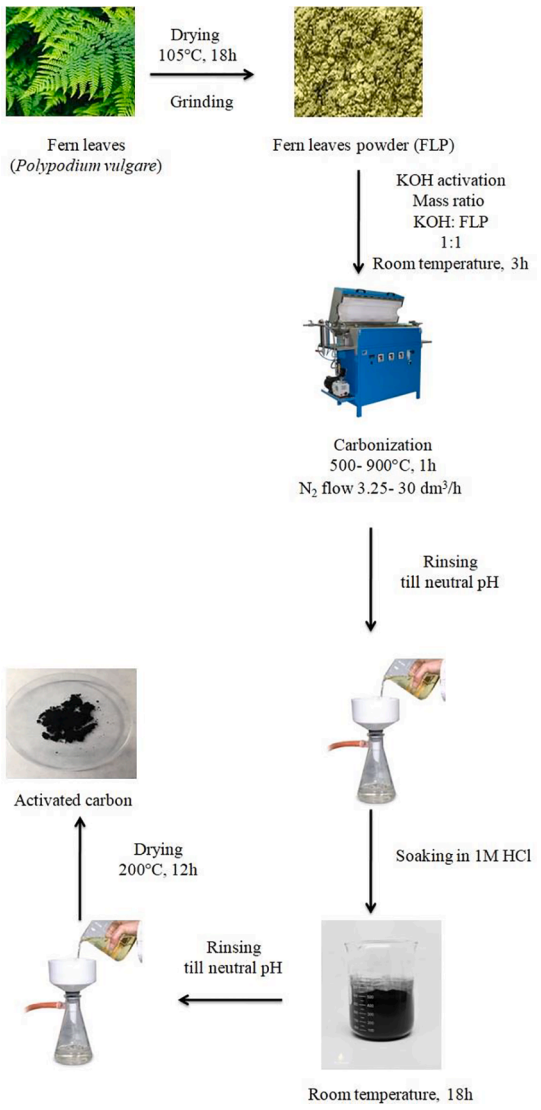


Fig. 1. Schematic illustration of the preparation of activated carbons from fern leaves (*Polypodium vulgare*).

nanoporous carbons. The common polypody was applied as a feedstock because it is widespread and can be and easy to grow and produce on a large scale. Moreover, it has not found any large-scale application yet. Common fern is widespread and easy to grow and produced on a large scale. Very high CO_2 adsorption at a pressure of 1 bar was achieved: 5.67 and 9.05 mmol/g at 298 and 273 K, respectively. According to our knowledge so, the high adsorption capacity was not reached up to now. The highest CO_2 adsorption was described by Rehman and Park [13] and was equal to 8.03 mmol/g at 273 K and 1 bar. Authors usually considered the influence of carbonization temperature on textural properties and CO_2 adsorption. Sometimes the importance of kind or amount of activating agent was discussed. We explore the significance of nitrogen flow during carbonization. We showed that the nitrogen flow is a very important parameter for tailoring the activated carbon properties.

2. Research methodology

Reagents used to synthesize activated carbons: potassium hydroxide and 35–38% hydrochloric acid, both purchased from Chempur Inc. Gases from Air Liquide Inc.: dinitrogen 5.0 and carbon dioxide 5.0.

2.1. Preparation of activated carbons from biomass

The leaves of the common fern (Polypodium vulgare) were used as a carbon precursor because it is a prevalent species, not covered by protection, occurring in Asia, North America, and Europe [36]. In this paper, to obtain activated carbons, a common fern from forests located in the West Pomeranian Voivodeship, Poland, was used.

The overall preparation scheme of activated carbons from fern leaves was shown in Fig. 1.. The leaves were dried at a temperature of 105 °C for 24 h and ground to powder. The powder was mixed with a saturated potassium hydroxide solution until it was homogeneous and left for 3 h at room temperature. The mass ratio of KOH to dry biomass was 1: 1. After 3 h, the sample was dried at 200° C for 18 h. The dry material was carbonized for 1 h. in the temperature range 500–900 ° C under nitrogen flow 3.25, 7.5, 15, 30 dm^3/h. The obtained activated carbon, containing the decomposition products of potassium hydroxide, was washed with distilled water until the pH was neutral. After the excess solution was evaporated, the material was treated with 1 mol/dm^3 HCl solution and left for 18 h. The carbon was then washed with distilled water until the chloride ion was completely eliminated. The final step was drying in an oven at 200° C for 16 h.

The samples were marked as follows: the first part of the name corresponding to the carbonization temperature, and the second one to the nitrogen flow. Thus, for example, 700_7.5 means a sample carbonized at 700 °C with a nitrogen flow of 7.5 dm^3/h.

3. Research methods

3.1. X-ray fluorescence spectroscopy

The Energy-dispersive X-ray fluorescence spectroscopy (EDXRF) was applied to measuring the elemental composition of the activated carbons. The instrument used was Epsilon 3 spectrometer from PANalytical B.V.

3.2. The percentage of ash content

Standards methods established the ash content (Ash%) (ASTM Designation D2866 11) [37]. Organic substances included in the activated carbons were burnt off and calcinated for three hours, at the temperature650 ± 25 °C in an electric muffle furnace.

3.3. X-ray diffraction (XRD)

Phase analysis of the activated carbons was performed using an X-ray diffractometer equipped with a copper lamp by PANalytical Empyrean. Phase identification was performed by analyzing the positions and intensities of the peaks observed in the diffractograms and comparing them with databases: ICDD PDF4 + 2015. The patterns were interpreted with X'Pert HighScore software.

The average crystallite thickness (L_c) and average graphene sheet diameter (L_a) can be approximately calculated using an expression derived by Scherrer [38]. As recommended by Liu et al. [39], for the dimension perpendicular to the average crystallite thickness (L_c), data for the (002) diffraction planes were used, where K equals 0.89. For the dimension in graphene sheet planes (L_a), (100/101) data were used, and K equals 1.84.

The number of graphitic layers (N) was estimated using the equation (1).

$$N = \frac{L_c}{d_{002}} \quad (1)$$

More details were provided in [14].

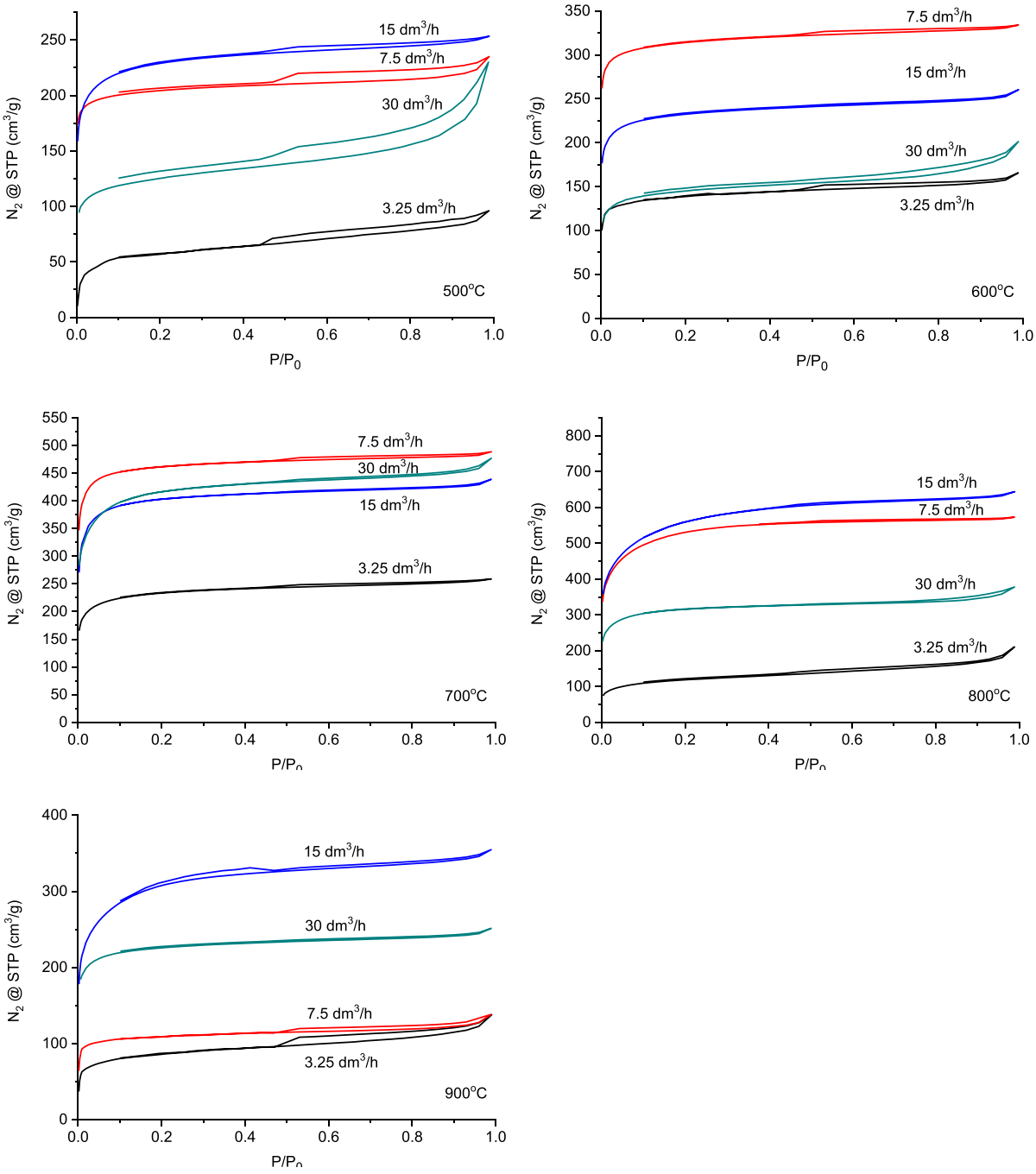


Fig. 2. Adsorption - desorption isotherms of nitrogen for activated carbons from common fern carbonized under various gas flows and temperatures.

3.4. Measurements of textural properties

The textural properties of the obtained activated carbons were characterized by nitrogen adsorption at 77 K and carbon dioxide adsorption at 298 K. The surface area and pore size analyzer Quadrasorb Evo supplied by Quantachrome Instruments was used for the measurements.

The samples' surface area (S_{BET}) was calculated with the Brunauer-Emmett-Teller (BET) equation in a relative pressure range of P/P_0 = 0.05 – 0.2. This range was narrowed down individually for each sample so that the straightness of the function (2) was met:

$$f\left(\frac{P}{P_0}\right) = \frac{1}{W\left(\frac{P}{P_0} - 1\right)} \tag{2}$$

where: W – a mass of gas adsorbed at a relative pressure (P/P_0), P – nitrogen pressure [mmHg], P_0 – 760 mmHg.

It is well known that Brunauer – Emmett - Teller equation is good for specific surface area calculation of macro- and mesoporous and nonporous materials and is used in P/P_0 range 0.05 – 0.3. It is obligatory to select the region of linearity for the BET plot within this range. The BET method is not appropriate in a strict sense for microporous materials [40,41]. If the common range P/P_0 is applied for microporous material isotherm, one often finds negative C constant (BET constant,

Table. 1
Textural properties of activated carbons obtained from common fern.

Activated carbon	S_{BET} [m^2/g]	V_{tot} [cm^3/g]	V_{mN2} [cm^3/g]	V_{mCO2} [cm^3/g]
500_3.25	187	0.157	0.139	0.103
500_7.5	629	0.364	0.332	0.490
500_15	714	0.393	0.363	0.203
500_30	475	0.357	0.301	0.150
600_3.25	430	0.257	0.233	0.186
600_7.5	1014	0.518	0.480	0.406
600_15	913	0.404	0.371	0.291
600_30	547	0.312	0.276	0.152
700_3.25	729	0.402	0.372	0.254
700_7.5	1420	0.758	0.705	0.453
700_15	1593	0.740	0.640	0.591
800_3.25	384	0.326	0.278	0.099
800_7.5	1994	0.881	0.825	0.408
800_15	1801	0.998	0.923	0.292
800_30	1216	0.586	0.531	0.366
900_3.25	278	0.214	0.185	0.118
900_7.5	429	0.214	0.189	0.163
900_15	1153	0.549	0.319	0.344
900_30	698	0.390	0.358	0.271

related to the energy of adsorption in the first adsorbed layer) and non-linearity of the BET plot.

Rouquerol et al. [42] reported that the BET equation could be applied for microporous materials only in the P/P_0 region where the curve showing the dependence of $V(1- P/P_0)$ on P/P_0 increases continuously and the C value is positive. In the case of our samples, the conditions laid down by Rouquerol et al. and linearity of the BET plot were met at a range P/P_0 from 0.05 to 0.2.

The total pore volumes (V_{tot}) were calculated from the nitrogen amount adsorbed at a relative pressure, P/P_0 of ≈ 1. The micropore volume (V_{mN2}) in the range of 1.4 – 2 nm was investigated via N_2 sorption and determined by the DFT method. The micropore volume (V_{mCO2}) in the range of 0.3 – 1.5 nm were analyzed via CO_2 sorption and also determined by the DFT method.

3.5. Raman spectroscopy

The Raman spectroscopy was utilized to determine the structure of the carbon framework of prepared carbon materials. The analyses were performed using an apparatus equipped with a CCD detector (Renishaw InVia). A laser (referred to as the red one) induced the material samples with a wavelength of 785 nm.

After normalization of the G peak maximum to 1, in each spectrum was assigned the intensity and location of the peaks G and D, and the ratio of these intensities was determined.

3.6. Scanning electron microscopy

The morphology of the obtained activated carbons was examined using the Hitachi SU 8200 scanning electron microscope with field emission (FE-SEM) equipped with detectors of secondary electrons (SE) and back-scattered electrons (BSE).

3.7. CO_2 and N_2 adsorption studies

The CO_2 and N_2 adsorption studies for all obtained activated carbons were carried out at the temperature of 298 K, to the pressure of 1 bar, using the Quantachrome Instruments Quadrasorb apparatus. Additionally, CO_2 adsorption was investigated at the temperature of 298 K, to the pressure of 1 bar.

Based on CO_2 adsorption tests up to 1 bar, the best sorbent was selected. Therefore CO_2 adsorption up to 30 bar pressure was carried out in the temperature range 273–353 K. The measurements were performed using the static volumetric method using the Hiden Isochema IMI – HTP Manometric gas sorption analyzer. More details about this method were described in [43].

4. Research results and discussion

4.1. Studies of textural properties by the adsorption of N_2 at temperature of 77 K and CO_2 temperature of 273 K

The nitrogen adsorption isotherms at temperature 77 K were shown in Fig. 2. All the isotherms were characterized by rapid growth at low-pressure P/P_0, which points that the activated carbons obtained from the common fern are microporous materials. The hysteresis loops for most of the samples were very narrow, sometimes even invisible, without proper magnification. The presence of the hysteresis loop indicates that mesopores also accompany the micropores. This phenomenon was established for activated carbons prepared under lower nitrogen flows (500 °C). Thus, it might conclude that these mild carbonization conditions are contributed to the mesopores. The most rapid growth of micropores was recorded for materials prepared under nitrogen flow equals 15 and 7.5 dm^3/h.

According to the IUPAC classification [44], all nitrogen adsorption isotherms which were presented in Fig. 2 except 900_15 represented Type Ia. The isotherm of activated carbon 900_15 was Type Ib. The ideal Ia and Ib isotherms are characterized by the relatively quick achievement of the adsorption limit, which results in the course of the adsorption isotherm parallel to the P/P_0 axis. The isotherms presented in Fig. 2 were parallel to the P/P_0 axis in the most range of P/P_0. Some of them were composite of Type I and II because of adsorption increase at high P/P_0 that indicated at the presence of a small amount of macropores. Detailed studies on macropores have not been carried out since these pores are not crucial for CO_2 adsorption. They are mainly used to transport the adsorbent from the outer surface to micro- and mesopores. Most of the isotherms were reversible, but for some of them, hysteresis was observed. The hysteresis was caused by capillary condensation that took place in mesopores. The sparse hysteresis loops were identified as H4 type, indicating slit pores.

Carefully analyzing the isotherms presented in Fig. 2 indicated that the hysteresis loops of activated carbons carbonized at flow equal to 30 cm^3/h at temperatures of 500 and 600 °C were extended to the lowest attainable pressures and were not closed. Although the effect of various factors on adsorption hysteresis is not fully understood, we can assume that these carbons have pores of complex shape and connectivity [45]. The purpose of the open hysteresis loops can be insufficient connectivity of the pore network, which inhibits desorption. The isotherms of 500_30 and 600_30 had differed from each other. Namely, the hysteresis was considerably brighter and the adsorption at high P/P_0 increased rapidly, indicating the presence of macropores as well. The micro- and micro/mesoporous network was not insufficiently developed at nitrogen flow of 30 dm^3/h. The shape and diameters of pores allows adsorption of nitrogen but the desorption was very slow.

Open low-pressure hysteresis may be associated with the swelling of a non-rigid porous structure or with the irreversible uptake of molecules in pores of about the same width as that of the adsorbate molecule or in some instances with an irreversible chemical interaction of the adsorbate with the adsorbent [46].

The textural properties of activated carbons obtained from common fern were compiled in Table 1.

It was found that during the carbonization of common fern: surface area, total pore volume, and micropore volume (determined by nitrogen adsorption) increases along with the increase of nitrogen flow. Once a certain maximum was reached; however, an increase in the N_2 flow decreased these values. Depending on the temperature, the flow value guaranteeing the maximization of the parameters mentioned above was 15 or 7.5 dm^3/h. A similar trend was observed for temperature changes with constant flow. With the nitrogen flow of 7.5 and 15 dm^3/h, the maximum values were obtained at the temperature of 800 °C. With a

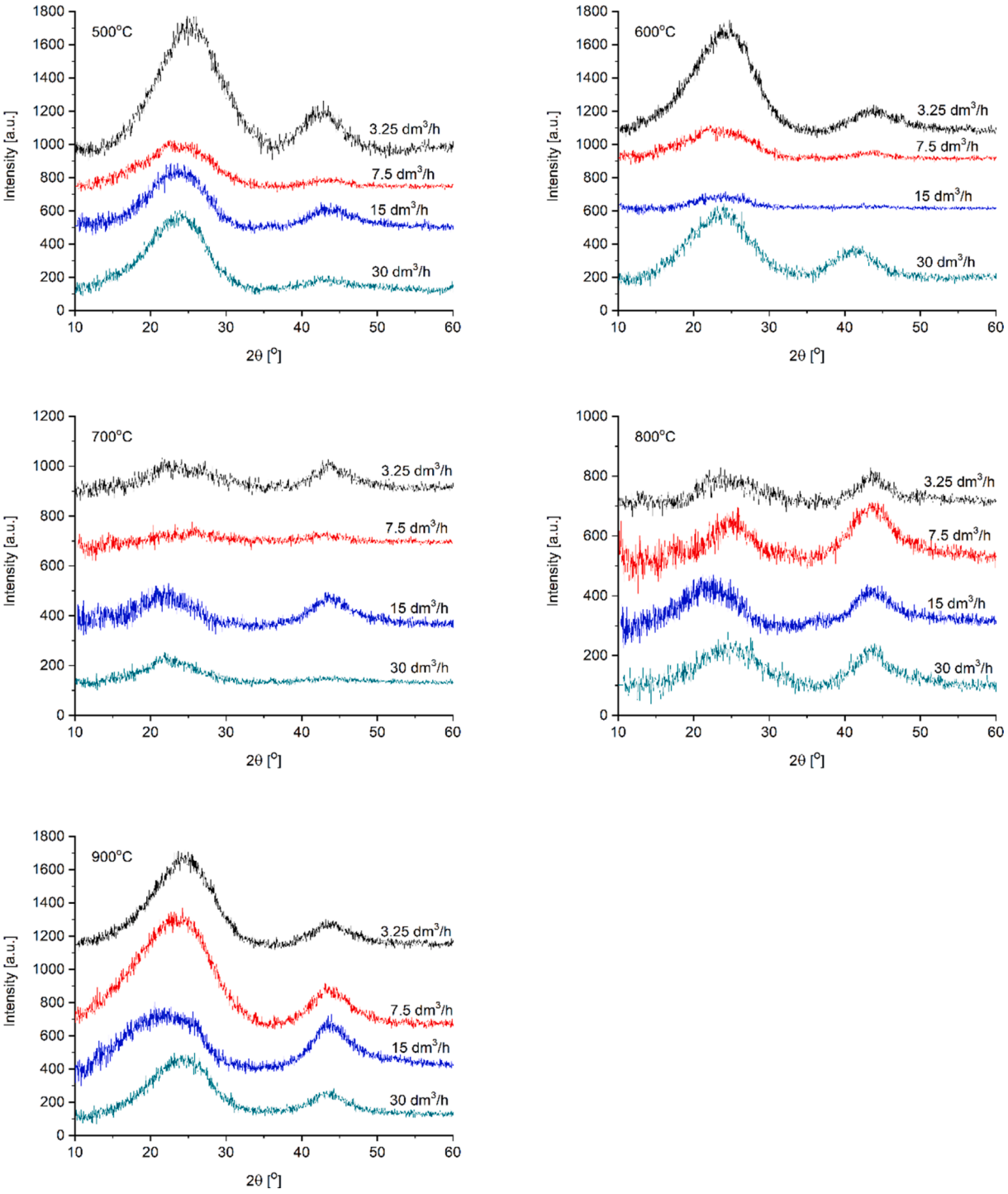


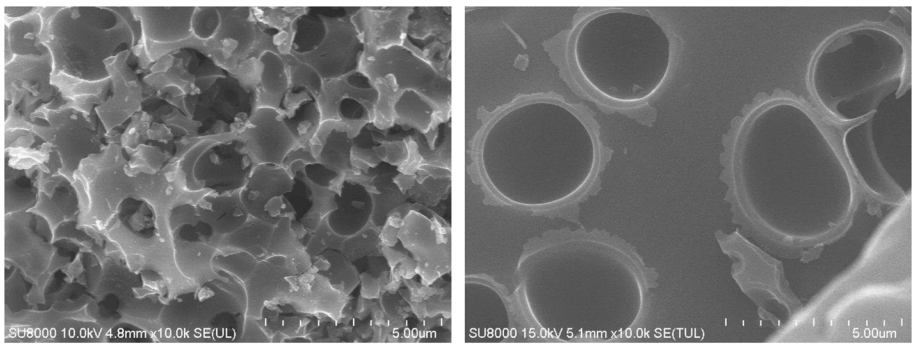
Fig. 3. Diffraction patterns of the activated carbons from common fern carbonized under various gas flows and temperatures.

nitrogen flow of 3.5 and 30 dm^3/h, the temperature of 700 °C turned out to be the most favorable.

The highest specific surface area was obtained for carbonized fern carbon at the temperature of 800 °C with a nitrogen flow of 7.5 dm^3/h (1994 m^2/g). The maximum volume of pores (0.998 cm3/g) and micropores determined by nitrogen adsorption (0.923 cm^3/g) was also achieved at this temperature, but with a nitrogen flow of 15 dm^3/h. Under this flow, carbon-containing most of all micropores was obtained. The micropores were determined by CO_2 adsorption (0.591 cm^3/g) but at a temperature of 700 °C.

The pore size distribution determined by the DFT method for the N_2 adsorption was shown in Fig. S 1. This method provides information concerning the pores with a 1.4 – 30 nm diameter range. However, the range below 6 nm is represented on the x-axis as no pores with larger diameters were observed.

Pores with diameters up to 3 nm dominated in common fern carbons (Fig. S 1) carbonized in nitrogen at all temperatures except 800 °C. With two exceptions: 2.25 dm^3 N_2/h and 500 °C and 7.5 dm^3 N_2/h and 700 °C. At the temperature of 800 °C, with average nitrogen flows: 75.5 and 15 dm^3/h, pores also formed in the range of 3–5.5 nm. In the high (30 dm^3/h) and low (3.25 dm^3/h) flow, the carbons with diameters not greater than 3 nm were obtained.



700_3.25 800_7.5

Fig. 4. Typical SEM images of activated carbons from common ferns.

CO_2 sorption isotherms were also used to calculate pore size distribution using the DFT method (Fig. S 2). The activated carbons obtained from the common fern contained micropores with four dominant ranges. The principal values in each of these ranges were: 0.350, 0.458, 0.523, and 0.823 nm. It should be noted that the share of pores with diameters of about 0.458 nm in the case of common fern carbon obtained with the flow of CO2 was negligible.

The main role of KOH was related to the oxidation of biomass. Potassium hydroxide reacts with part of the carbon and stimulates the formation of the pores, especially micropores and small mesopores, during the carbonization combined with the activation process. So it is no surprise that the carbonization temperature had an influence on the textural properties of the activated carbons. The increase in temperature causes an increase in the reaction rate, so the increase in temperature influenced the development of micropores and an increase in the value of structural parameters. However, after exceeding a certain limit value, in this case 700 °C, unfavorable destruction of the microporous structure took place and these values decreased.

KOH also removed impurities such as SiO_2 and dissolved the tar by-products. Chemical reactions between the biomass and KOH occurred during the carbonization combined with chemical activation. Carbon oxidation led to potassium carbonate, hydrogen, metallic potassium, water, and carbon oxide. The main reactions of biomass and KOH were as follows:

$$4\ KOH + C \rightarrow K_2CO_3 + H_2O + 2H_2$$

$$6\ KOH + 2C \rightarrow 2\ K_2CO_3 + 2\ K + 3\ H_2$$

$$2\ KOH + C + H_2O \rightarrow K_2CO_3 + 2H_2$$

$$2\ KOH + 2C \rightarrow 2CO + 2\ K + H_2$$

The functional groups present in the biomass also decomposed into volatile substances such as carbon oxide, carbon dioxide, and water.

Due to the formation of gaseous products during carbonization and the reaction of these products with biomass, the flow of inert gas - nitrogen became an essential parameter. Its flow rate influenced the speed of removing gaseous products from the reaction zone and the eliminating or intensification of their interaction with the carbon source.

4.2. XRD method

Graphite structure and purity of activated carbons were characterized by means of XRD. The diffraction patterns of the activated carbons obtained from common fern were shown in Fig. 3.

All the diffraction patterns do not show reflections characteristic of potassium compounds. Therefore, it can assume that the KOH used to activate the carbons has been completely removed. The diffraction patterns of all materials show only poorly developed reflections at angles 2θ equal to 23 and 43°, which correspond to the plane (002) and (100/101) of the graphite structure. Broad peaks indicate a highly disordered carbon structure. The order of the obtained carbons was assessed by comparing the presented reflexes with the corresponding planes of graphite.

By analyzing the XRD patterns, it was observed that relatively high intensities characterized the materials obtained at the two lowest temperatures (500 and 600 °C) and the highest (900 °C) temperature under the lowest (3.25) and the highest (30) nitrogen flow. This proves a relatively higher degree of ordering of these materials. The most disordered activated carbons were formed at average carbonization temperatures and average flow values. The influence of the nitrogen flow rate at 700 and 800 °C on the ordering of the carbon structure was feeble.

An attempt was also made to assess the degree of ordering of the obtained carbons using Scherrer equation [47] (La and Lc: average graphene sheet diameter and average crystallite thickness respectively), Bragg law [47] (d_{002}: average spacing between graphitic layers). The number of graphitic layers (N) was estimated using the equation (1). A detailed description of the equations was provided in [14].

The Scherrer equation was derived for carbons with a high degree of graphitization, but it can also be used for carbons with a non-ordered structure to roughly estimate the quantities characterizing crystallites and conduct a comparative analysis [48].

The values of average spacing between graphitic layers, average crystallite thickness, average Graphene sheet diameter, and an average number of graphitic layers are presented in Tab. S 1.

The average interlayer spacing was about 0.381 nm, which is approximately a 12% increase compared to that of highly ordered graphite. The spacing range was from 0.3654 to 0.4090 nm.

The higher inter-planer distance for activated carbons may be caused by the sp^3 defects and/or by interlayer repulsion between the negatively charged surfaces because of surface functional groups [49]. The values of interlayer spacing and the width of the peaks corresponding to (002) and (101) reflection planes indicated the presence of disordered carbon structure [9]. For some materials, the values of d-spacing were not calculated because the peak corresponding to (002) reflection planes was not observed. These were materials with the highest disordering.

The crystallite sizes, along with the plane perpendicular to the graphene layers, were small (2.623–3.616 nm), which gave the small number of graphitic layers in the crystallites from 1.7 to 2.5. The average crystallite sizes along the graphitic plane were within the range of 0.670–0.952 nm.

The values presented in Tab. S 1 confirmed the conclusions derived from Fig. 3 that activated carbons synthesized at the lowest and the highest temperatures and using the lowest and the highest nitrogen flows showed relatively higher crystallinity. In addition, these activated carbons exhibited the highest average crystallite thickness along the c axis, average Graphene sheet diameter, and the average number of

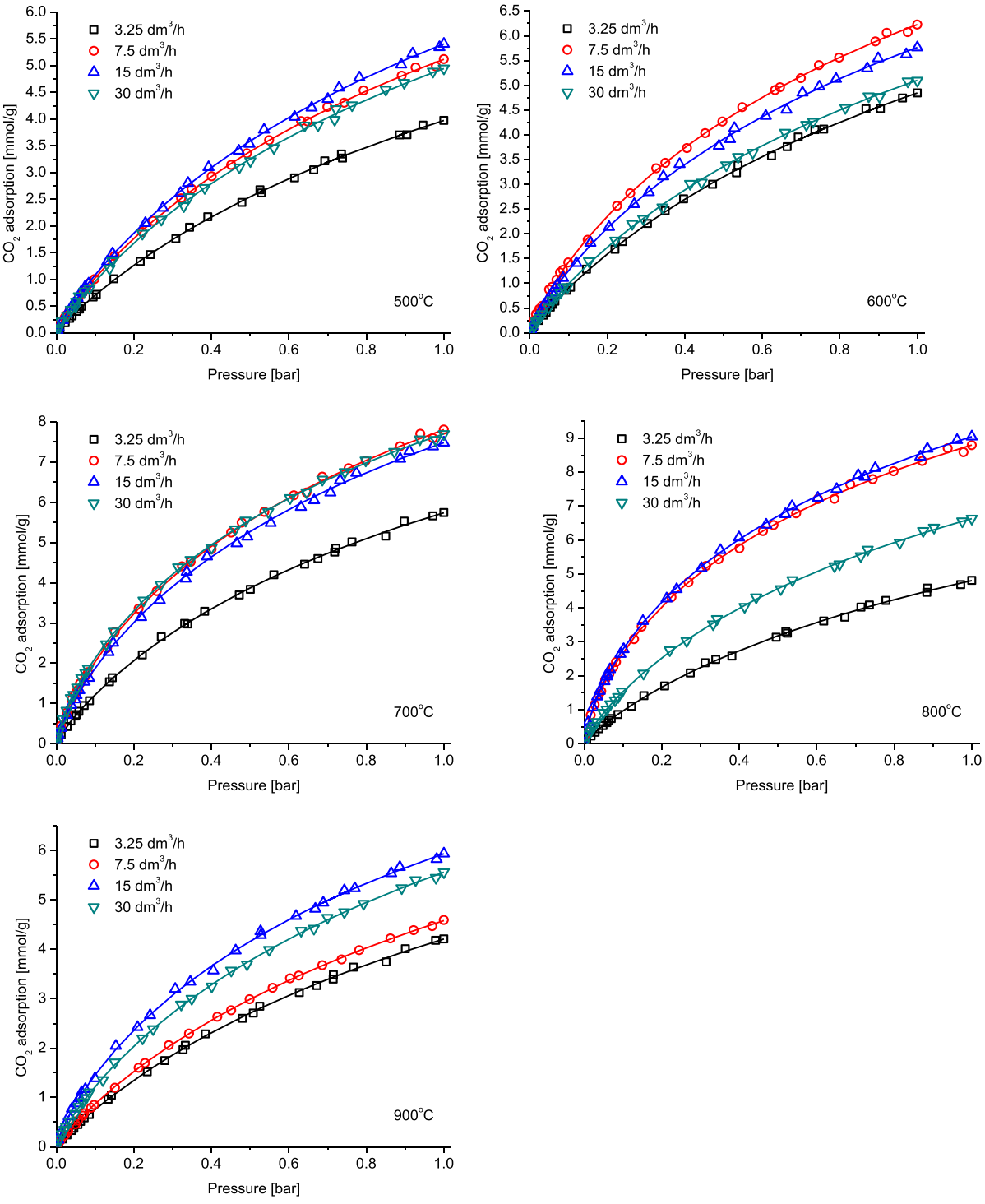


Fig. 5. CO_2 adsorption isotherms at 273 K for activated carbons from common fern carbonized at different temperatures and different gas flow Symbols marked experimental data, and lines marked the data determined from the Sips equation.

graphitic layers.

4.3. Raman spectroscopy

The Raman spectra of activated carbons were characterized by the presence of a wide frequency range of 1300 – 1600 cm^{-1}. The peak named D (Disorder) was centered around 1300 cm^{-1}. Its presence was attributed to breathing vibrations with the A1g symmetry of the aromatic ring of carbons. Moreover, its intensity was proportional to the short-range disorder of the carbon structure. The peak located about 1580 cm^{-1} is called the G (Graphitic) band. The E2g stretching vibrations of all sp2 carbon pairs came from the rings and chains. Its intensity was related to the arrangement of the carbon structure [50].

A determination of the correlation between the location of the bonds G and D and their intensities (IG/ID) allowed to determine the ordering of carbon structure. An increase of the value of the intensity ratio of the

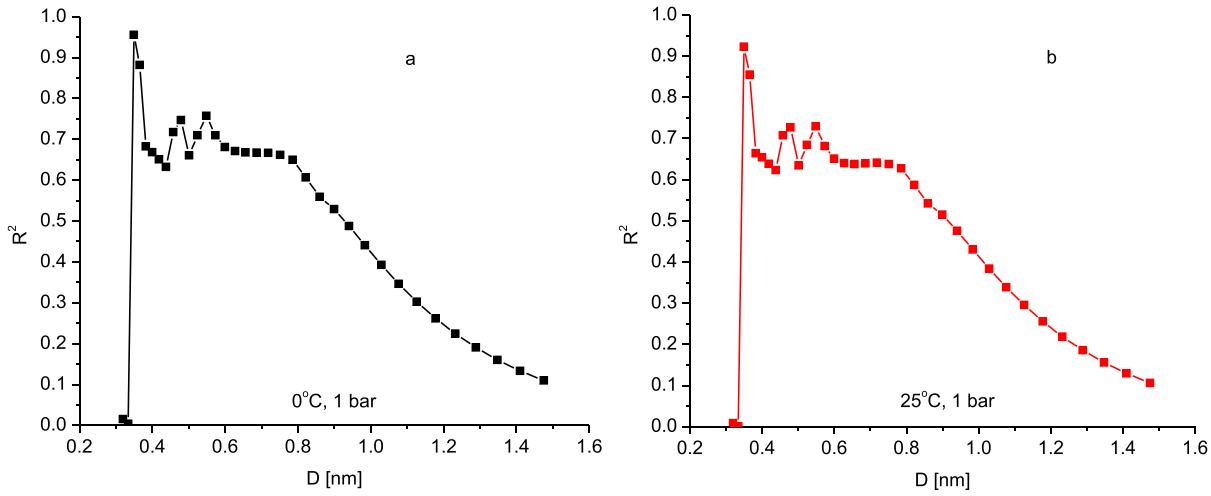


Fig. 6. Dependence of the R^2 correlation coefficient on the pore diameter at the temperatures of (a) 273 and (b) 298 K.

IG/ID peaks indicateed a higher degree of graphitization of the carbon [51].

The Raman spectra were presented in Fig. S 3. All tested activated carbons had two characteristic bands in the frequency range around 1580 cm^{-1} (G band) and around 1300 cm^{-1} (D band). The spectra were smoothed by the Fourier Transform method to reduce noise and then normalized to unity by dividing by the maximum value for a given sample. For all materials, the maximum intensity value was observed for the D peak. Thus, after normalizing the spectra, the intensity value of the G peak simultaneously corresponded to the IG / ID ratio. On the basis of Fig. S 3. the values of the IG/ID ratios obtained from Raman spectroscopy were compiled in Tab. S 1. It was found that the values of the IG/ID ratios for all the activated carbons tested were very close to each other and they are in a range from 0.522 to 0.725. All values of the IG/ID ratios were lower than unity, which proves the high disorder of the structure of the obtained materials.

Higher values of the IG/ID ratios were observed for samples obtained at lower and higher temperatures and at the lowest and highest nitrogen flows. An analysis of the carbon materials by means of Raman spectroscopy has been confirmed the results of XRD studies. The most disordered materials were formed at medium temperatures, and nitrogen flows. For comparison, of the two methods Fig. S 4 shows the changes in L_c with temperature and gas flow. It can be clearly seen that the tendency to change IG / ID and Lc along with the above-mentioned parameters is similar.

4.4. SEM method

The SEM images presented below were typical for the given sample. A series of micrographs were taken for each material, and those that were most representative of a given activated carbon were selected. It was considered advisable to present all the materials at the same magnification. A magnification of 10,000 times was found to be the best.

Quite large granules containing mostly macropores were observed. Low visibility of macropores was found at the lowest temperature: 500 °C and the highest: 900 °C. In Fig. 4. were shown typical SEM images of activated carbons from common fern. The other micrographs were compiled in the appendix (Fig. S 5. SEM pictures of activated carbons prepared at temperature of 500oCFig. S5 - Fig. S9).

4.5. The elemental analysis

In order to determine the purity of the samples, the ash content in activated carbons was determined. The ash is the residue that remains after the combustion process. The ash content indicates the quality of activated carbons, affects the pore volume and surface area. The high ash content leads to the clogging of pores and reducing surface area and pore volume. The figures show the effect of carbonization temperature and gas flow on the ash content. The average ash content was 4.3 wt%, and the highest value was 5.78 wt%.

The ash content has been depended on the carbon combustion and efficient removal of inorganic compounds due to reaction with KOH during carbonization connected with chemical activation. For example, SiO_2 reacting with KOH formed water-soluble K_2SiO_3, which was removed during the purification step.

The increase in carbonization temperature decreased the ash content in the case of both precursors. It can be assumed that the reason was the formation of more water-soluble compounds at higher temperatures.

It can be assumed that the increase in carbonization temperature in combination connected with chemical activation led to a faster reaction of inorganic matter with KOH. The rate of reaction of inorganic compounds increased more with temperature than the rate of carbon combustion.

The lowest ash content was obtained with the nitrogen flow of 7.5 dm^3/h. Both the lower and the higher nitrogen flow were associated with an increase in the ash content.

The ash content values were consistent with the XRF results Tab. S 2. All the carbons contained trace amounts of potassium, but it should be noted that this element is present in the starting materials, i.e., dry common fern. The presence of calcium, manganese, silicon, copper, iron, magnesium, zinc, sulfur, and chlorine were also identified. The rich elemental composition of activated carbons from common fern may be surprising, but similar results were also obtained by Smirti et al. [52].

4.6. Studies on CO_2 adsorption

All activated carbons obtained from common ferns were analyzed in terms of the CO_2 adsorption. The tests were carried out at a temperature of 273 and 298 K, up to 1 bar pressure. The results are shown in Fig. 5 and Fig. S 11.

For all activated carbons, CO_2 adsorption isotherms at temperatures 273 and 298 K indicate a similar course. They were characterized by a quick increase at low pressure combined with a relatively quick increase at higher pressure. CO_2 adsorption capacities obtained at 1 bar pressure at temperatures 273 and 298 K are presented in Tab. S 3. A significant influence of nitrogen flow on CO_2 adsorption was found. The activated carbons carbonized under nitrogen flow equal to 3.25 dm^3/h demonstrated the lowest CO_2 uptake. The rising nitrogen flows up to 7.5 or 15 dm^3/h allowed to obtain the activated carbons characterized by one of the highest CO_2 adsorption. Further increase of this parameter up to 30

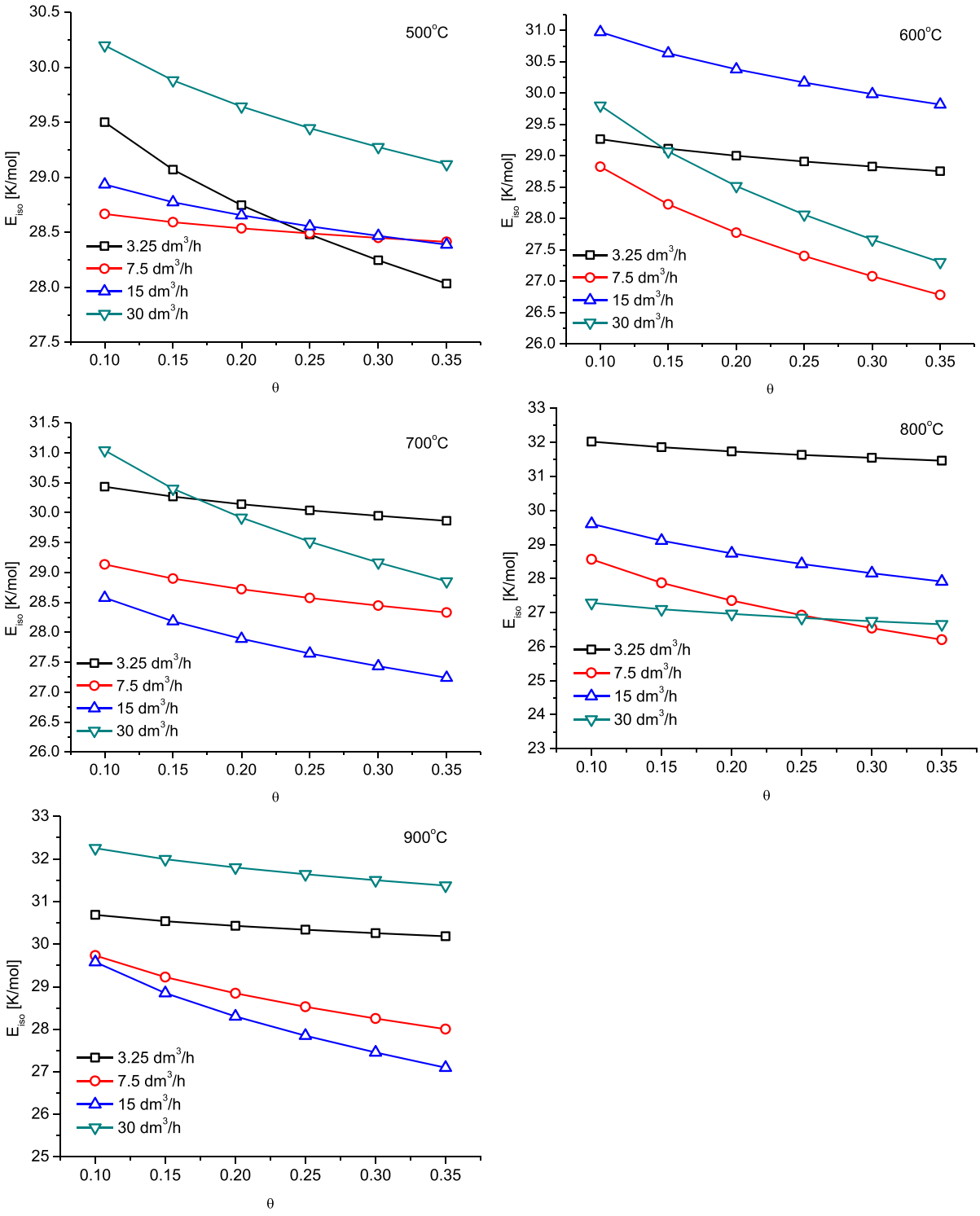


Fig. 7. The isosteric heat of adsorption for the activated carbons carbonized at various temperatures and under different gas flow rates calculated on the basic of CO_2 adsorption measurements at temperatures of 273 and 298 K.

dm^3/h has been caused a decrease in the CO_2 capacity. The most favorable carbonization temperature in terms of CO_2 adsorption turned out to be 800 and 700 °C.

For activated carbons obtained from the common fern, the highest CO_2 adsorption at 1 bar pressure was achieved for activated carbon obtained at 800 °C under a nitrogen flow of 15 dm^3/h. The adsorption of CO_2 at 1 bar pressure on activated carbon named 800_15 amounted to 5.67 and 9.05 mmol/g, for 298 and 273 K, respectively. The CO_2 adsorption capacities that were obtained for carbons prepared from biomass were very high and were among the highest values described in the literature. For all activated carbons, the CO_2 uptake was higher at a temperature of 273 K than at a temperature of 298 K. Along with an increase in the temperature, the decrease in the adsorption of CO_2 was observed. Such a phenomenon confirms the physical adsorption connected with a slightly exothermic effect. The van der Waals forces play a fundamental role in the interaction between CO_2 particles and the

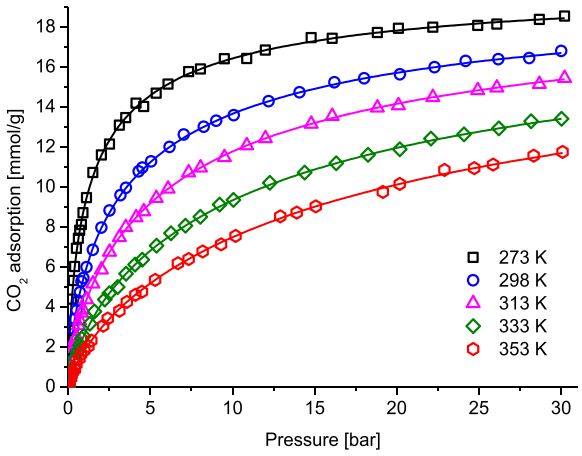


Fig. 8. Isotherms of the CO_2 adsorption on the 800_15 activated carbon up to 30 bar of Symbols marked experimental data, and lines marked the data determined from the Sips equation.

Table. 2
The parameters of the Sips model, the standard errors, the correlation coefficients for 800_15 activated carbon at different temperatures.

T [K]	q_m [mmol/g]	b [bar^{-1}]	n	SE (q_m)	SE(b)	SE(n)	R^2
273	20.62	0.782	0.701	0.11	0.010	0.008	0.9996
298	20.51	0.382	0.718	0.13	0.004	0.007	0.9998
313	20.39	0.251	0.736	0.16	0.003	0.007	0.9998
333	20.28	0.15	0.754	0.33	0.003	0.011	0.9995
353	20.17	0.100	0.772	0.46	0.002	0.011	0.9997

activated carbons. These molecular forces are quite strong at low temperatures, whereas the decrease in the temperature caused their weakness. It is in agreement with Le Chatelier's principle.

Typical composition of exhaust gases is nitrogen (70–75 vol%.), carbon dioxide (15–16 vol%) and water (5–7 vol%) [52]. The exhaust gas pressure equals 1 bar. Therefore, it is desirable to find an excellent CO_2 sorbent at low pressures, especially at 0.15 bar. Under these conditions, obtained activated carbons indicate quite high CO_2 adsorption as well. At a temperature of 298 K, and under 0.15 bar, adsorption on sample 800_15 amounts to 1.71 mmol/g. This uptake was among the highest values reported in the literature.

The plots showing the dependence of CO_2 uptake on the specific surface area (Fig. S 12), total pore volume (Fig. S 13), and micropore volume (determined through nitrogen adsorption) (Fig. S 14) were performed to analyze the influence of textural parameters on CO_2 adsorption on activated carbons at the temperatures of 273 and 298 K under 1 bar pressure.

The comparison of the R^2 correlation coefficients obtained from Fig. S 12 - Fig. S 14 found that the best correlation between CO_2 adsorption at 273 K was obtained in the case of micropore volumes. Based on this motion, it can be concluded that the value of CO_2 adsorption at a pressure of 1 bar at 273 K depended on the micropores volume from the range of 1.4–2 nm.

The highest R^2 correlation coefficient for plotted dependencies at 298 K was found for the total pore volume for studied activated carbons. The same factor that was obtained from the CO_2 adsorption at 298 K versus the specific surface area plot was also very high and differed from the highest values by 1.1 and 1.7%.

Some authors have found that the most important issue for CO_2 adsorption up to 1 bar was small micropores tested through CO_2 adsorption. Therefore, an acute analysis was carried out to examine the correlation between CO_2 adsorption at 1 bar pressure, at temperatures of 273 and 298 K, and the pore volume smaller than the specified diameter ranging from 0.3300 – 0.334 nm and ending with 0.300–1.475 nm. Fig. 6 shows the R^2 correlation coefficient as a function of the pore diameter.

Fig. S 15 shows the CO_2 adsorption at 1 bar versus the total pore volume of pores for which the highest values of the R^2 correlation coefficient were obtained. Based on the CO_2 adsorption at the temperature of 298 K, the highest R^2 correlation coefficient equals 0.9543 was found for the pores from the range 0.330 – 0.349 nm. Thus, it should be recognized that the pores obtained on the CO_2 adsorption had no effect on CO_2 adsorption, or perhaps the result was more complicated.

The experimental CO_2 adsorption isotherms (Fig. 5 and Fig. S 11) were analyzed utilized: Langmuir, Freundlich, Sips, Toth, UNILAN, Radke-Prausniz, and Fritz-Schlunder equations presented in Supplementary materials. The isotherms parameters were obtained by nonlinear regression analysis. The least-squares method was used to assess the quality of fitting models to experimental data. The best fit for all activated carbons guaranteed the Sips equation (at 273 and 298 K temperatures). The parameters of the Sips model (q_m,b, n), the Standard errors (SE), and the R^2 correlation coefficients altogether are compiled in Tab. S 4 and Tab. S 5. Symbols marked experimental data, and lines marked the data determined from the Sips equation. It can be clearly seen, that a very good fit of the model to the experimental data was gained. The values of standard errors and correlation coefficients as well confirm this. The Sips model is commonly used for the description of heterogeneous adsorbents, e. g. activated carbons.

The isosteric heat of adsorption (Q_{iso}) is a significant parameter to characterize the connections between adsorbent and adsorbate. It provides information about the strength of adsorption. The higher value of the isosteric heat of adsorption indicates the stronger interaction between adsorbent and adsorbate. Moreover, the higher the isosteric heat of adsorption, the higher cost of the regeneration is.

The isosteric heat of adsorption was determined based on the differentiated form of the Clausius-Clapeyron equation:

$$\ln(p)_\theta = \frac{Q_{iso}}{R}\frac{1}{T} + C \tag{3}$$

whereQ_{iso} – the isosteric heat of adsorption under constant surface coverage degree [kJ/mol]R – Cas constant [J/mol·K]θ– surface coverage degree

The pressure values for the given surface coverage degree were calculated by rearranged Sips equation:

$$\mathrm{p} = \left(\frac{\theta}{b_S - \theta \cdot b_S}\right)^{\frac{1}{n_S}} [bar] \tag{4}$$

Taking into account that

$$\theta = \frac{q}{q_{mS}} \tag{5}$$

The parameter from the Sips model were taken from Tab. S 4Tab. S 5. The adsorption isostere for the temperatures of 273 and 298 K were prepared i. e. the dependence between $\ln(p)_\theta$ and 1/T. Based on the slopes of the straight lines, the values of the isosteric heat of adsorption were determined for all activated carbons. These values, as a function of the surface coverage degree, were shown in Fig. 7.

The isosteric heat of adsorption amounted from the range 26.5–32.5 kJ/mol for the surface coverage degree ranging from 0.1 to 0.35. These values strongly confirm the physical character of the CO_2 sorption on the activated carbons. The isosteric heat of adsorption was decreasing along with the increase of the surface coverage degree. The higher the surface coverage degree is, then, the weaker interaction between the CO_2 and activated carbons. The CO_2 is bound to the surface of the activated carbons by the van der Waals forces; furthermore, it can be easily desorbed.

Recent studies indicated that if the gas contains only CO_2, the most efficient are sorbents characterized by the isosteric heat of adsorption of

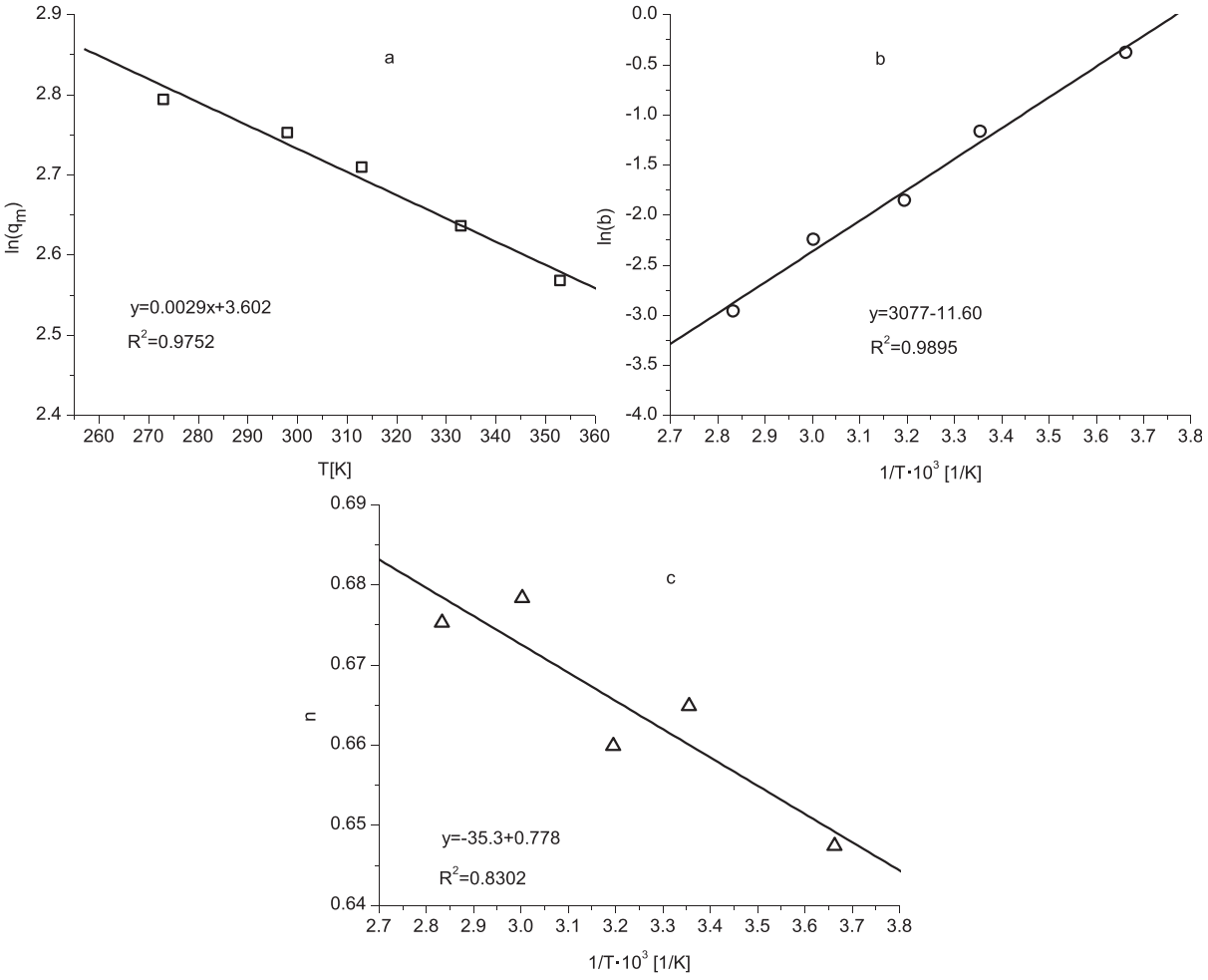


Fig. 9. The plots used to calculation of the Sips equations (4–6) for the 800_15 activated carbon; (a) ln(qm) versus T, (b), ln(b) versus 1/T, (c) n versus 1/T.

Table. 3
The parameters of the Sips model from Eqs. 4–6 for 800_15 activated carbon.

Parameter	Value	Unit	SE
Q	26,499	J/mol	99
b_0	0.260	bar^{-1}	0.031
n_0	0.692		0.004
α	0.362		0.009
q_{m0}	20.66	mmol/g	0.21
γ	0.086		0.019

CO_2 from the range 22−28 kJ/mol. Moreover, sorbents for the CO_2 adsorption from flue gases should have the CO_2 heat of adsorption from 26 to 31 kJ/mol. The CO_2 heat of adsorption for all studied activated carbons fulfilled these requirements. These values are very desirable because they are connected with low adsorbents regeneration costs.

The calculated values of the isosteric heat of adsorption should be approached with some caution because they were obtained based on data collected at two temperatures, i.e., isosteres were drawn, taking into account only two points. However, it can be assumed that this is a reasonably reliable estimate.

For the best adsorbent - the activated carbon named 800_15, the CO_2 adsorption up to 30 bar, and the temperature range 273−353 K was studied (Fig. 8). The highest value of the CO_2 uptake equals 18.56 mmol/g was achieved under 30 bar, and at the temperature of 273 K.

The isotherms parameters were obtained by nonlinear regression

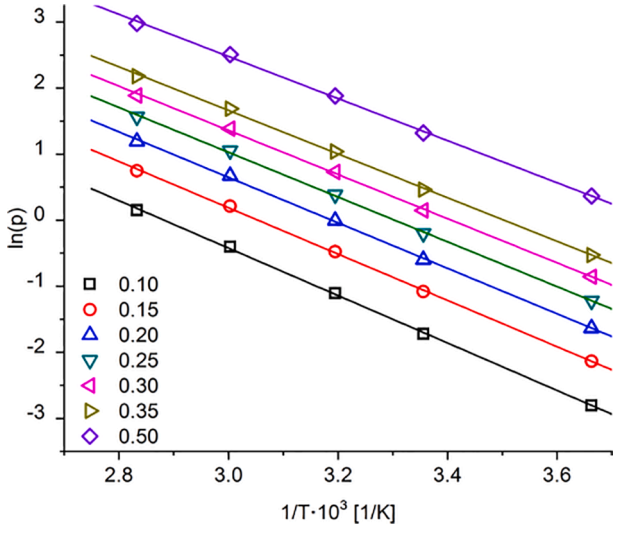


Fig. 10. Isosteres of the adsorption for the different surface coverage degree (the 800_15 activated carbon).

analysis, again. The least-squares method was used to assess the quality of fitting models to experimental data. The best fit for the activated carbons was given by the Sips equation. The parameters of the Sips

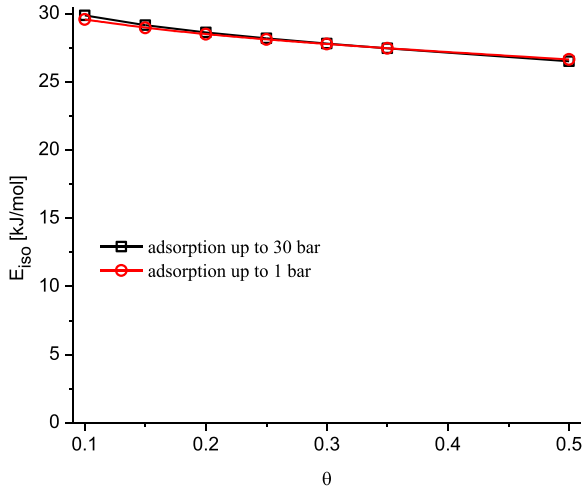


Fig. 11. The isosteric heat of adsorption as a function of the surface coverage degree for the 800_15 activated carbon based on the N_2 adsorption up to 1 and 30 bar.

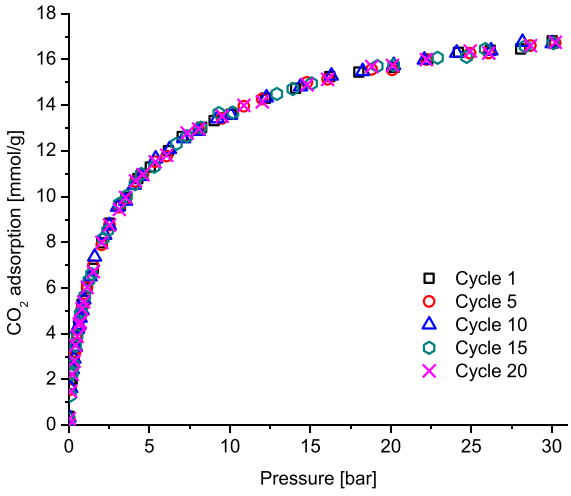


Fig. 12. Multi-cycles isotherms for the 800_15 activated carbon at 298 K, 1st, 5th, 10th, 15th, 20th adsorption isotherm.

model, the Standard errors (SE), and the R^2 correlation coefficients for all temperatures are gathered in Table 2. Collected data confirmed an excellent model fitting to the experimental data.

The parameters of the Sips model depend on the temperature as following:

$$q_{mS} = q_{m0} \cdot exp\left[\chi\left(1 - \frac{T}{T_0}\right)\right] \tag{6}$$

$$b_S = b_0 exp\left[\frac{Q}{RT}\left(\frac{T_0}{T} - 1\right)\right] \tag{7}$$

$$n_S = n_0 + \alpha\left(1 - \frac{T_0}{T}\right) \tag{8}$$

whereq_{mo}, χ, Q, b_0, n_0, α are constants

T_0 – reference temperature

The lowest adsorption temperature, i.e., 273 K was chosen as the reference temperature, as it is recommended. The Q parameter is synonymous with the isosteric heat of adsorption at the surface coverage degree equals 0.5 ($Q = (Q_{iso})_{\theta=0.5}$)

To determine q_{mo} and χ, b_0 and Q, n_0 and α, the plots showing the dependencies between ln(q_m) and temperature, ln(b) and 1/T, n and 1/T were shown in Fig. 9, respectively.

The parameters of the Sips model from Eqs. 4–6, which defined the dependence amongst q_{mS}, b_S, n_S, and the temperature were compiled in Table 3.

The values of the isosteric heat of adsorption for the 800_15 activated carbon were calculated in the same way as for all activated carbons for which the CO_2 adsorption up to 1 bar pressure was studied. However, there is one difference: the adsorption isosteres were obtained for five different temperatures from the range 273–353 K.

The adsorption isosteres at different surface coverage degrees for the 800_15 activated carbon were shown in Fig. 10 .

Based on the slopes of the obtained linear functions from Fig. 10 the isosteric heats of adsorption were calculated. In turn, Fig. 11 demonstrates the comparison of both: the isosteric heat of the high-pressure adsorption (at five different temperatures) and the low-pressure adsorption (at two temperatures) as a function of the surface coverage degree.

It was evidenced that the values of the isosteric heat of adsorption based on the two temperatures only, were very similar to the values obtained from five different temperatures. Thus these values can be considered as reliable. At the surface coverage degree amounted to 0.5, the isosteric heat of adsorption equals 26.49 kJ/mol (Fig. 11), and this value is in agreement with the isosteric heat of adsorption determined from eq. (5) and presented in Tab. 3 (26.50 kJ/mol).

For all adsorbents, their stability and maintaining constant adsorption capacity after many regeneration cycles are crucial. Therefore, the re-usability of the 800_15 activated carbon was studied by performing twenty adsorption–desorption runs at a temperature of 298 K. 1st, 5th, 10th, 15th, 20th adsorption isotherms were presented in Fig. 12. After twenty cycles, there were no changes in CO_2 adsorption. The highest standard deviation equals 0.10. On this basis, it can be concluded that the 800_15 activated carbon is a highly stable CO_2 sorbent. It can be regenerated many times without losing its useful ability for CO_2 adsorption.

4.7. Studies of the CO_2 over N_2 selectivity

Apart from CO_2, flue gas includes N_2. Therefore, one of the criteria for selecting the best sorbent is CO_2 over N_2 selectivity. Thus, nitrogen adsorption measurements at 298 K, up to 1 bar pressure, were applied for several activated carbons from the fern. The results of N_2 adsorption studies are shown in Fig. S 16. The N_2 uptake obtained on activated carbons from fern was below 0.30 mmol/g.

Based on the CO_2 and N_2 adsorption isotherms at 298 K, a quantitative analysis of the CO_2 over N_2 selectivity was carried out.

The selectivity ratio of CO_2 over N_2 at 298 K under p pressure was calculated according to Eq. (9) (the quotient of the uptake of CO_2 to N_2):

$$S_{CO_2/N_2} = \frac{q_{CO_2(p)}}{q_{N_2(p)}} \tag{9}$$

The selectivity ratio of CO_2 over N_2 was rapidly decreased along with the pressure increased up to 0.2 bar (Fig. 13 and Fig. S 17).

The highest selectivity ratio of CO_2 over N_2 equals 823 was achieved under the 0.01 bar for the 500_3.25 activated carbon, while under 1 bar, it was only 42. The selectivity ratios of CO_2 over N_2 for the best sorbents named 800_7.5 were 718 and 23, respectively. The values of CO_2/N_2 selectivity ratios at 1 bar pressure at 298 K were high (15.8–42.0). The highest values of CO_2/N_2 selectivity ratios were significantly higher than those described in the literature.

The theoretical selectivity for the typical content of flue gas was also elaborated using the Ideal Adsorption Solution Theory (Eq. (10)) and

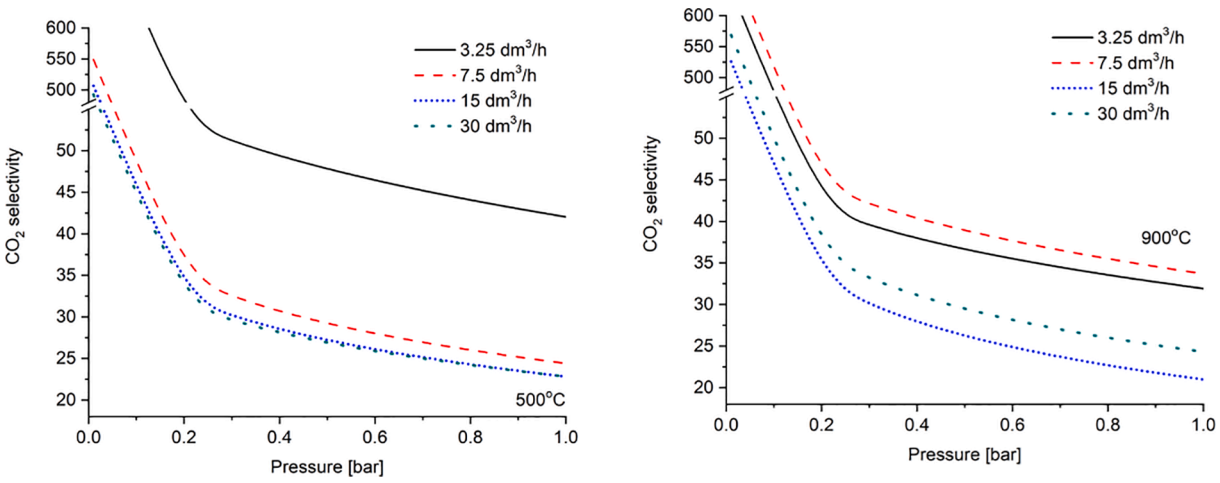


Fig. 13. The CO_2 over N_2 selectivity as a function of pressure at 298 K and different gas flow.

Table. 4
The selectivity ratios of CO_2 over N_2 calculated by using the Ideal Adsorbed Solution Theory.

Activated carbon	S_{IAST}
500_3.25	75.9
500_7.5	50.6
500_15	46.8
500_30	45.5
600_3.25	58.0
600_7.5	52.6
600_15	53.6
600_30	50.6
700_3.25	52.0
700_7.5	51.1
700_15	50.8
700_30	53.7
800_3.25	50.2
800_7.5	66.3
800_15	59.5
800_30	52.3
900_3.25	59.3
900_7.5	63.3
900_15	48.5
900_30	52.5

their values were compiled in Table 4. This method is commonly used to predict components in the gas mixture adsorption based on the single gas adsorption data.

$$S_{IAST} = \frac{q_{CO_2}@p_{CO_2}/q_{N_2}@p_{N_2}}{p_{N_2}/p_{CO_2}} \quad (10)$$

Where:q_j @ p_i – adsorption capacity of i at pressure p_i

The IAST method allowed to calculate the CO_2 over N_2 selectivity for a typical exhaust gas composition, i. e. $p_{N2} = 0.85$ and $p_{CO2} = 0.15$. The S_{IAST} values obtained for activated carbons from ferns ranged from 45.5 to 75.9. These values were considerably higher than for activated carbons derived from different biomass sources.

5. Conclusions

The studies were focused on the possibility of preparation of activated carbons from the common polypody for the purpose of obtaining the materials with enhanced CO_2 adsorption. The influence of carbonization temperature and gas flow on the porous structure of obtained carbons have been examined. The experimental results demonstrated that these parameters have a significant influence on the textural properties, what is associated with the CO_2 adsorption capacities by obtained materials. It has been evidenced that the largest values of specific surface area, pore volume, and micropores attained activated carbons synthesized in the temperature range of 800–850 °C under nitrogen flow of 7.5–15 dm^3/h.

The CO_2 uptake under a pressure of 1 bar depended on: the micropores volume at the temperature of 273 K and the specific surface area at the temperature of 298 K. An increase in these parameters caused an increase in the CO_2 adsorption. Moreover, the adsorption selectivity of CO_2 over N_2 depended on the total pore volume: an increase in the total pore volume at the temperature of 298 K under a pressure of 1 bar caused a decrease in the adsorption selectivity of CO_2 over N_2 because of a simultaneous increase in the N_2 adsorption.

However, obtained activated carbons exhibited a high value of the adsorption selectivity of CO_2 over N_2. In addition, the achieved CO_2 heat values were within the ranges recommended for both pure CO_2 sorption and CO_2 sorption from flue gases.

The best fitting to the experimental data for all activated carbons at all temperatures by a comparison of the values of errors functions was achieved with the application of the Sips equation.

Activated carbon synthesized from common polypody at the temperature of 800 °C, under nitrogen flow of 15 dm^3/h, at the mass ratio of KOH to precursor equal to 1 atteined the largest CO_2 adsorption. At the temperature of 298 K and under the pressure of 1 bar, the CO_2 adsorption was 5.67 mmol/g, and the selectivity coefficient was 23. The S_{IAST} selectivity was 59.5. These values are very high, which makes this material a promising CO_2 sorbent.

Based on the performed investigations it was found that abovementioned parameters correspond with most of the requirements for an ideal CO_2 sorbent. In addition, the activated carbons obtained from the common polypody are stable CO_2 sorbents. They can be regenerated many times by lowering the pressure without losing the ability to adsorb CO_2.

Declaration of Competing Interest

The authors declare that they have no known competing financial interests or personal relationships that could have appeared to influence the work reported in this paper.

Appendix A. Supplementary data

Supplementary data to this article can be found online at https://doi.org/10.1016/j.cej.2021.131751.

References:

[1] Z. Li, L. Sellaoui, D. Franco, M.S. Netto, J. Georgin, G.L. Dotto, A. Bajahzar, H. Belmabrouk, A. Bonilla-Petriciolet, Q. Li, Adsorption of hazardous dyes on functionalized multiwalled carbon nanotubes in single and binary systems: experimental study and physicochemical interpretation of the adsorption mechanism, Chem. Eng. J. 389 (2020) 124467, https://doi.org/10.1016/j.cej.2020.124467.

[2] S. Wjihi, F. Aouaini, A. Erto, M. Balsamo, A.B. Lamine, Advanced interpretation of CO2 adsorption thermodynamics onto porous solids by statistical physics formalism, Chem. Eng. J. 406 (2021) 126669, https://doi.org/10.1016/j.cej.2020.126669.

[3] M. Wang, A. Lawal, P. Stephenson, J. Sidders, C. Ramshaw, W. Hill, B. Park, S. Sn, Chemical engineering research and design post-combustion CO2 capture with chemical absorption: a state-of-the-art Preview, Chem. Eng. Res. Des. 89 (2010) 1609–1624, https://doi.org/10.1016/j.cherd.2010.11.005.

[4] A. Gęsikiewicz-Puchalska, M. Zgrzebnicki, B. Michalkiewicz, U. Narkiewicz, A. W. Morawski, R.J. Wrobel, Improvement of CO2 uptake of activated carbons by treatment with mineral acids, Chem. Eng. J. 309 (2017) 159–171.

[5] J. Li, B. Michalkiewicz, J. Min, C. Ma, X. Chen, J. Gong, E. Mijowska, T. Tang, Selective preparation of biomass-derived porous carbon with controllable pore sizes toward highly efficient CO_2 capture, Chem. Eng. J. 360 (2019) 250–259, https://doi.org/10.1016/j.cej.2018.11.204.

[6] J. Serafin, A.K. Antosik, K. Wipliszewska, Z. Czech, Preparation of Activated Carbon from the Biodegradable film for CO2 Capture Applications, Polish, J Chem. Technol. 20 (2018) 75–80, https://doi.org/10.2478/pjct-2018-0041.

[7] J. Kapica-Kozar, B. Michalkiewicz, R.J. Wrobel, S. Mozia, E. Piróg, E. Kusiak-Nejman, J. Serafin, A.W. Morawski, U. Narkiewicz, Adsorption of carbon dioxide on TEPA-modified TiO2/titanate composite nanorods, New. J. Chem. 41 (16) (2017) 7870–7885.

[8] A. Hart, N. Gnanendran, Cryogenic CO2 capture in natural gas, Energy Procedia 1 (1) (2009) 697–706, https://doi.org/10.1016/j.egypro.2009.01.092.

[9] C.E. Powell, G.G. Qiao, Polymeric CO2/N2 gas separation membranes for the capture of carbon dioxide from power plant flue gases, J. Membr. Sci. 279 (1–2) (2006) 1–49, https://doi.org/10.1016/j.memsci.2005.12.062.

[10] L. Keshavarz, M. reza ghaani, J. M. Don MacElroy, N. J. English, A comprehensive review on the application of aerogels in CO2-adsorption: Materials and characterization, Chem. Eng. J. 412 (2021) 128604. https://doi.org/10.1016/j.cej.2021.128604.

[11] H. Yuan, J. Chen, D. Li, H. Chen, Y. Chen, 5 Ultramicropore-rich renewable porous carbon from biomass tar with excellent adsorption capacity and selectivity for CO_2 capture, Chem. Eng. J. 373 (2019) 171–178, https://doi.org/10.1016/j.cej.2019.04.206.

[12] A. Rehman, S.-J. Park, Tunable nitrogen-doped microporous carbons: Delineating the role of optimum pore size for enhanced CO_2 adsorption, Chem. Eng. J. 362 (2019) 731–742, https://doi.org/10.1016/j.cej.2019.01.063.

[13] J. Serafin, M. Baca, M. Biegun, E. Mijowska, R.J. Kalenczuk, J. Sreńscek-Nazzal, B. Michalkiewicz, B., Direct conversion of biomass to nanoporous activated biocarbons for high CO2 adsorption and supercapacitor applications, Appl. Surf. Sci. 497 (2019), 143722, https://doi.org/10.1016/j.apsusc.2019.143722.

[14] J. Sreńscek-Nazzal, U. Narkiewicz, A.W. Morawski, R. Wróbel, R.A. Gęsikiewicz-Puchalska, B. Michalkiewicz, Modification of commercial activated carbons for CO2 adsorption, Acta Phys. Pol. A 129 (2016) 394–401, https://doi.org/10.12693/APhysPolA.129.394.

[15] J. Serafin, M. Ouzzine, O.F.C. Junior, J. Sreńscek-Nazzal, Biomass & Bioenergy, Preparation of low-cost activated carbons from amazonian nutshells for CO2 storage, 144 (2021) 105925. https://doi.org/10.1016/j.biombioe.2020.105925.

[16] D. Dokur, S. Keskin, Effects of force field selection on the computational ranking of MOFs for CO2 separations, Ind. Eng. Chem. Res. 57 (6) (2018) 2298–2309, https://doi.org/10.1021/acs.iecr.7b0479210.1021/acs.iecr.7b04792.s001.

[17] M. Miyamoto, S. Ono, K. Kusukami, Y. Oumi, S. Uemiya, High water tolerance of a core–shell-structured zeolite for CO2 adsorptive separation under wet conditions, ChemSusChem 11 (11) (2018) 1756–1760, https://doi.org/10.1002/cssc.201800063.

[18] A. Rehman, S.J. Park, Preparation and characterization of polyamides and nitrogendoped carbons for enhanced CO2 capture, Bull. Korean Chem. Soc. 38 (11) (2017) 1285–1292, https://doi.org/10.1002/bkcs.2017.38.issue-1110.1002/bkcs.11281.

[19] J. Kapica-Kozar, E. Pirog, E. Kusiak-Nejman, R.J. Wróbel, A. Gęsikiewicz-Puchalska, A.W. Morawski, U. Narkiewicz, B. Michalkiewicz, Titanium dioxide modified with various amines used as sorbents of carbon dioxide, New. J. Chem. 41 (4) (2017) 1549–1557, https://doi.org/10.1039/C6NJ02808J.

[20] I. Yanase, T. Maeda, H. Kobayashi, The effect of addition of a large amount of CeO2 on the CO2 adsorption properties of CaO powder, Chem. Eng. J. 327 (2017) 548–554, https://doi.org/10.1016/j.cej.2017.06.140.

[21] J. Feng, H. Guo, S. Wang, Y. Zhao, X. Ma, Fabrication of multi-shelled hollow Mg-modified CaCO3 microspheres and their improved CO2 adsorption performance, Chem. Eng. J. 321 (2017) 401–411.

[22] N.P. Wickramaratne, M. Jaroniec, Activated carbon spheres for CO2 adsorption, ACS Appl. Mater. Interfaces 5 (5) (2013) 1849–1855, https://doi.org/10.1021/am400112m.

[23] L. Luo, T. Chen, Z. Li, Z. Zhang, W. Zhao, M. Fan, Heteroatom self-doped activated biocarbons from fir bark and their excellent performance for carbon dioxide adsorption, J CO2 Util. 25 (2018) 89–98, https://doi.org/10.1016/j.jcou.2018.03.014.

[24] G. Srinivas, V. Krungleviciute, Z.-X. Guo, T. Yildirim, Exceptional CO2capture in a hierarchically porous carbon with simultaneous high surface area and pore volume, Energy & Environmental Science. 7 (1) (2014) 335–342, https://doi.org/10.1039/C3EE42918K.

[25] J. Wang, Y. Lin, Q. Yue, K. Tao, C. Kong, L. Chen, N-rich porous carbon with high CO2 capture capacity derived from polyamine-incorporated metal–organic framework materials, RSC Advance. 6 (58) (2016) 53017–53024, https://doi.org/10.1039/C6RA09472D.

[26] S. Xian, F. Xu, Z. Zhao, Q. Xia, J. Xiao, Y. Li, H. Wang, Z. Li, A novel carbonized polydopamine (C-PDA) adsorbent with High CO2 adsorption capacity and water vapor resistance, AIChE Journal. 62 (10) (2016) 3730–3738, https://doi.org/10.1002/aic.v62.1010.1002/aic.15283.

[27] H. Gao, Y. Sun, J. Zhou, R. Xu, H. Duan, Mussel-inspired synthesis of polydopamine-functionalized graphene hydrogel as reusable adsorbents for water purification, ACS Appl Mater Interfaces. 5 (2) (2013) 425–432, https://doi.org/10.1021/am302500v.

[28] J.W. To, J. He, J. Mei, R. Haghpanah, Z. Chen, T. Kurosawa, S. Chen, W.G. Bae, L. Pan, J.B. Tok, J. Wilcox, Z. Bao, Hierarchical N-doped carbon as CO2 adsorbent with High CO2 selectivity from rationally designed polypyrrole precursor, J. Am. Chem. Soc. 138 (3) (2016) 1001–1009, https://doi.org/10.1021/jacs.5b1195510.1021/jacs.5b11955.s001.

[29] V. Chandra, S.U. Yu, S.H. Kim, Y.S. Yoon, D.Y. Kim, A.H. Kwon, M. Meyyappan, K. S. Kim, Highly selective CO2 capture on N-doped carbon produced by chemical activation of polypyrrole functionalized graphene sheets, ChemComm. 48 (5) (2012) 735–737, https://doi.org/10.1039/C1CC15599G.

[30] T. Ben, Y. Li, L. Zhu, D. Zhang, D. Cao, Z. Xiang, X. Yao, S. Qiu, Selective adsorption of carbon dioxide by carbonized porous aromatic framework (PAF), Energy Environ. Sci. 5 (8) (2012) 8370, https://doi.org/10.1039/c2ee21935b.

[31] B. Ashourirad, P. Arab, T. Islamoglu, K.A. Cychosz, M. Thommes, H.M. El-Kaderi, A cost-effective synthesis of heteroatom-doped porous carbons as efficient CO2 sorbents, J Mater. Chem. A. 4 (38) (2016) 14693–14702, https://doi.org/10.1039/C6TA06251B.

[32] J. Wang, A. Heerwig, M.R. Lohe, M. Oschatz, L. Borchardt, S. Kaskel, Fungi-based porous carbons for CO2 adsorption and separation, J. Mater. Chem. 22 (2012) 13911–13913, https://doi.org/10.1039/C2JM32139D.

[33] J. Fujiki, K. Yogo, The increased CO2 adsorption performance of chitosan-derived activated carbons with nitrogen-doping, Chem. Commun. 52 (1) (2016) 186–189.

[34] Y. Li, G. Ruan, A.S. Jalilov, Y.R. Tarkunde, H. Fei, J.M. Tour, Biochar as a renewable source for high-performance CO2 sorbent, Carbon 107 (2016) 344–351, https://doi.org/10.1016/j.carbon.2016.06.010.

[35] A.R. Smith, K.M. Pryer, E. Schuettpelz, P. Korall, H. Schneider, P.G. Wolf, A Classification for extant ferns, Taxon 55 (3) (2006) 705–731, https://doi.org/10.2307/25065646.

[36] ASTM D2866 – 11 Standard Test Method for Total Ash Content of Activated Carbon.

[37] Cullity B.D., StockS.R., Elements of X-Ray Diffraction, New York, 19788.

[38] L. Lu, V. Sahajwalla, C. Kong, D. Harris, Quantitative X – ray diffraction analysis and its application to various coals, Carbon 39 (12) (2001) 1821–1833, https://doi.org/10.1016/S0008-6223(00)00318-3.

[39] Lowell S., Shields J., Thomas M.A., Thommes M., Characterization of Porous Solids and Powders: Surface Area, Porosity, and Density, Particle Technology Series Springer Netherlands, ISBN 1-4020-2302-2, 16 (2004) 347.

[40] S.J. Gregg, K.S.W. Sing, Adsorption, surface area and porosity, academic press, London (1982), https://doi.org/10.1002/bbpc.19820861019.

[41] J. Rouquerol, P. Llewellyn, F. Rouquerol, Is the BET equation applicable to microporus adsorbents?Characterisation of porouys solids, Studies in Surface Science and Catalysis 160 (2007) 49–56, https://doi.org/10.1016/S0167-2991(07)80008-5.

[42] J. Sreńscek-Nazzal, U. Narkiewicz, A.W. Morawski, R.J. Wróbel, B. Michalkiewicz, Comparison of optimized isotherm models and error functions for carbon dioxide adsorption on activated carbon, J. Chem. Eng. Data 60 (11) (2015) 3148–3158, https://doi.org/10.1021/acs.jced.5b00294.

[43] M. Thommes, K. Kaneko, V.A. Neimark, J.P. Oliver, F. Rodriguez-Reinoso, J. Rouquerol, K.S.W. Sing, Physisorption of gases, with special reference to the evaluation of surface area and pore size distribution (IUPAC Technical Raport, Pure Appl. Chem. 87 (2015) 1051–1069, https://doi.org/10.1515/pac-2014-1117.

[44] K. Bratek, W. Bratek, M. Kułażyński, Carbon adsorbents from waste ion exchange resins, Carbon 40 (12) (2002) 2213–2220, https://doi.org/10.1016/S0008-6223(02)00091-X.

[45] K.S.W. Sing, D.H. Everett, R.A.W. Haul R.A.W, L. Moscou, R.A. Pierotti, J. Rouquerol, T. Siemienewska, Reporting physisorption data for gas solid systems with special reference to the determination of surface – area and porosity. Pure Appl. Chem., 57 (1985) 603 – 619. https://doi.org/10.1351/pac198557040603.

[46] B.D. Cullity, S.R. Stock, Elements of X-ray diffraction, Addison-Wesley, Reading, MA, 1978, p. 828.

[47] B.S. Girgis, Y.M. Temerk, M.M. Gadelrab, I.D. Abdullah, X – ray diffraction patterns of activated carbons prepared under various conditions, carbon, Science 8 (2) (2007) 95–100, https://doi.org/10.5714/CL.2007.8.2.095.

[48] A. Ghosh, C. Amaral Razzino, A. Dasgupta, K. Fujisawa, L.H.S. Vieira, S. Subramanian, R.S. Costa, A.O. Lobo, O.P. Ferreira, J. Robinson, M. Terrones, H. Terrones, B.C. Viana, Structural and electrochemical properties of babassu coconut mesocarp – generated activated carbon and few – layer graphene, Carbon 145 (2019) 175–186, https://doi.org/10.1016/j.carbon.2018.12.114.

[49] A.C. Ferrari, J. Robertso, Raman spectroscopy of amorphous, nanostructured, diamond – like carbon, and nanodiamond, Phil. Trans. R. Soc. Lond. A 362 (1824) (2004) 2477–2512, https://doi.org/10.1098/rsta.2004.1452.

[50] J. Robertson, Diamond – like amorphous carbon, Materials Science and Engineering R 37 (2002) 129–281, https://doi.org/10.1016/S0927-796X(02)00005-0.
[51] S. Chettri, S. Manivannan, V.R. Muddarsu, Nutrient and elemental composition of wild edible ferns of the Himalaya, Am. Fern J. 108 (3) (2018) 95–106, https://doi.org/10.1640/0002-8444-108.3.95.
[52] J.C.Y. Ng, W.H. Cheung, G. McKay, Equilibrium studies of the sorption of Cu(II) ions onto chitosan, J. Colloid Interf. Sci. 255 (1) (2002) 64–74, https://doi.org/10.1006/jcis.2002.8664.